Acta Cryst. (1994). **D50**, 75–84

Crystal Structure of Chloromuconate Cycloisomerase from *Alcaligenes eutrophus* JMP134 (pJP4) at 3 Å Resolution

BY H. HOIER*

Institut für Organische Chemie und Isotopenforschung der Universität Stuttgart, Pfaffenwaldring 55, 70569 *Stuttgart, Germany*

M. SCHLÖMANN AND A. HAMMER

Institut für Mikrobiologie der Universität Stuttgart, Allmandring 31, 70569 *Stuttgart, Germany*

J. P. GLUSKER AND H. L. CARRELL

Institute for Cancer Research, The Fox Chase Cancer Center, Philadelphia, PA 19111, *USA*

A. GOLDMAN

Centre for Biotechnology, PO Box 123, *Turku, SF*-20521, *Finland*

J. J. STEZOWSKI

Department of Chemistry, University of Nebraska Lincoln, Lincoln, NE 68588-0304, *USA*

AND U. HEINEMANN†

Institut für Organische Chemie und Isotopenforschung der Universität Stuttgart, Pfaffenwaldring 55, 70569 *Stuttgart, Germany*

(*Received* 7 *May* 1993; *accepted* 24 *August* 1993)

Abstract

Chloromuconate cycloisomerase (E.C. 5.5.1.7) is an enzyme involved in the 2,4-dichlorophenoxyacetate degradation pathway of *Alcaligenes eutrophus* JMP134 (pJP4). The crystal structure of this protein was determined at 3 Å resolution by molecular-replacement techniques using atomic coordinates from the reported crystal structure of the homologous muconate cycloisomerase (E.C. 5.5.1.1) from *Pseudomonas putida* as the search model (42% identical positions in the sequences). Structure refinement by simulated-annealing and restrained least-squares techniques converged at $R = 0.195$. In the crystals studied, space group $I4$, the protein is present as two octamers per unit cell with two subunits per asymmetric unit. Each subunit consists of two globular domains, one of which forms an α/β-barrel. Comparison of this structure with that of muconate cycloisomerase reveals the reasons for the altered substrate specificity of chloromuconate cycloisomerase. Marked differences are observed in polarity, accessibility and hydrogen-bonding potential in the channel leading into the active site as well as in the active center itself.

Introduction

Generally, chloro-substituted aromatic compounds are degraded comparatively slowly and often incompletely. Some bacteria, however, have adapted to the utilization of chloroaromatics such as chlorophenoxyacetates, chlorophenols, chlorobenzoates, chlorobenzenes and others (Engesser & Fischer, 1991; Häggblom, 1992; Schlömann, 1992). In many cases these growth substrates are initially converted to chlorocatechols which are then further degraded *via* the modified 3-oxoadipate pathway (modified *ortho*-cleavage pathway). On this catabolic route the chlorocatechols are subject to intradiol dioxygenation giving rise to the corresponding chlorosubstituted *cis,cis*-muconates (Fig. 1). The latter are cycloisomerized to dienelactones which, compared to the corresponding intermediates of the 3-oxoadipate pathway, carry an additional double bond, because the cycloisomerization is coupled to chloride elimination. The dienelactones are finally funnelled into

* Author to whom correspondence should be addressed. Present address: Laboratory of Biophysical Chemistry, University of Groningen, Nijenborgh 4, 9747 AG Groningen, The Netherlands.

† Present address: Institut für Kristallographie, Freie Universität Berlin, Takustrasse 6, 14195 Berlin, Germany.

the normal 3-oxoadipate pathway by hydrolytic and reductive reactions.

A characteristic feature of most enzymes of the modified *ortho*-cleavage pathway is their range of substrates. The chlorocatechol 1,2-dioxygenases of various chloroaromatic utilizing strains and, in addition, the chloromuconate cycloisomerase (CMCI) of *Pseudomonas* sp. B13, have a low specificity; they also convert chloro- and methyl-substituted compounds (Dorn & Knackmuss, 1978; Schmidt & Knackmuss, 1980; Pieper, Reineke, Engesser & Knackmuss, 1988). In contrast, the CMCI of *Alcaligenes eutrophus* JMP134 has a remarkably high specificity (Kuhm, Schlömann, Knackmuss & Pieper, 1990). While 2,4-dichloro-*cis,cis*-muconate is a very good substrate, the affinity for *cis,cis*-muconate is extremely low. Similarly, 2-chloro-*cis,cis*-muconate is converted slowly and with a high K_m, so that this compound is excreted into the medium when *A. eutrophus* JMP134 is grown in the presence of 3-chlorobenzoate (Pieper, Knackmuss & Timmis, 1993).

Another interesting feature of the chloromuconate cycloisomerases is their capability of dehalogenating chloro-substituted muconates. This property, in the case of 3-chloro- and 2,4-dichloro-*cis,cis*-muconate, might be a necessary consequence of the reaction mechanism (Fig. 2; Ngai & Kallen, 1983; Schlömann, Fischer, Schmidt & Knackmuss, 1990), implying that chloride elimination is gratuitous. Dehalogenation during 2-chloro-*cis,cis*-muconate cycloisomerization, however, was recently found to

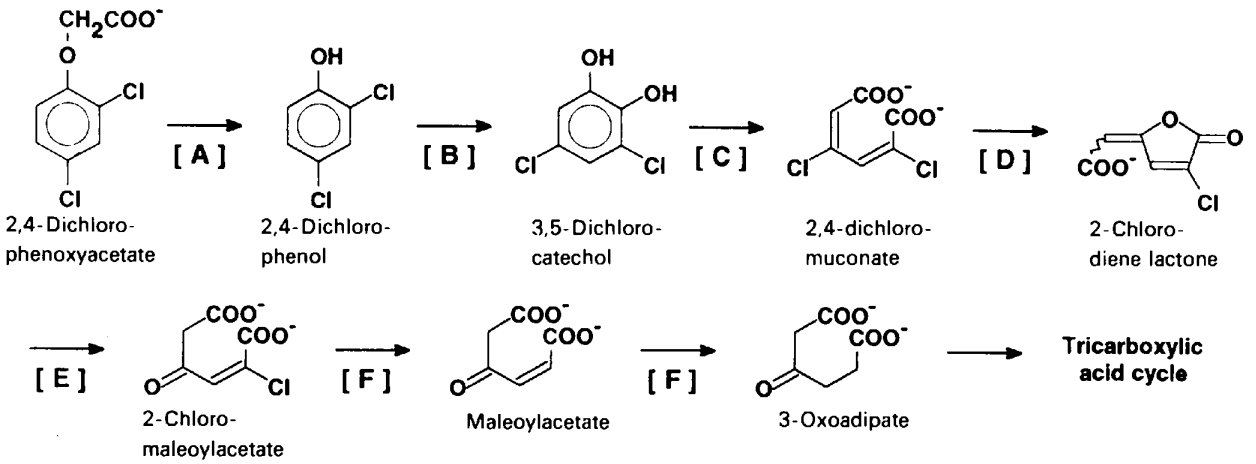

Fig. 1. Modified 3-oxoadipate pathway for 2,4-dichlorophenoxyacetate in *Alcaligenes eutrophus* JMP134. Abbreviations: *A* = 2,4-dichlorophenoxyacetate/α-ketoglutarate dioxygenase, *B* = dichlorophenol hydroxylase, *C* = chlorocatechol 1,2-dioxygenase, *D* = chloromuconate cycloisomerase, *E* = dienelactone hydrolase, *F* = maleoylacetate reductase.

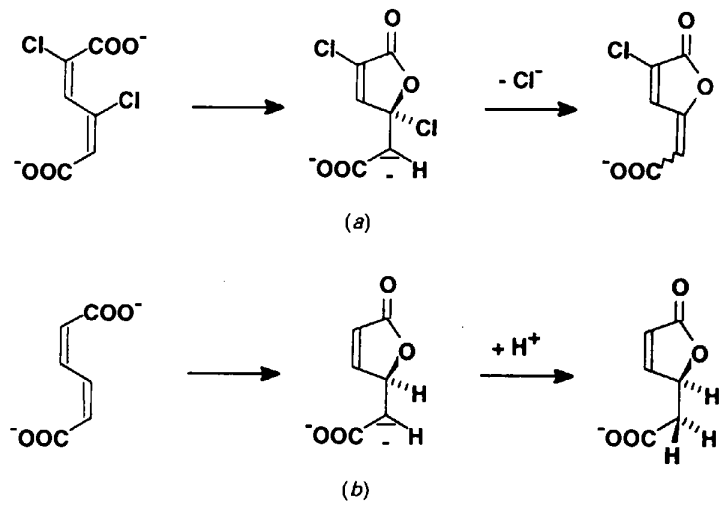

Fig. 2. Cycloisomerization of (*a*) 2,4-dichloro-*cis,cis*-muconate and (*b*) *cis,cis*-muconate.

be neither a spontaneous reaction as originally reported (Schmidt & Knackmuss, 1980) nor a gratuitous enzyme-catalyzed reaction. This conclusion is based on the observation that chloromuconate cycloisomerases can cleave the carbon–chlorine bond, but this capability is not present in normal muconate cycloisomerases (Vollmer & Schlömann, 1993).

Considerable information has already been reported for the muconate cycloisomerase (MCI, often also named muconate lactonizing enzyme, MLE) of *Pseudomonas putida*. The enzyme catalyzes a *syn* addition to a double bond (Fig. 2), a reaction which invokes a carbanion as an intermediate (Avigad & Englard, 1969; Ngai & Kallen, 1983; Kozarich, Chari, Ngai & Ornston, 1986). Muconate cycloisomerase is an octamer of identical 40 kDa subunits (Aldrich, Frantz, Gill, Kilbane & Chakrabarty, 1987) and has been shown to be an α/β-barrel protein (Goldman, Ollis & Steitz, 1985, 1987).

The amino-acid sequence of the pJP4-encoded CMCI, as predicted from its DNA sequence (Ghosal & You, 1989; Perkins, Gordon, Caceres & Lurquin, 1990), shows 42% identity to that of the MCI from *P. putida* (Fig. 3, Aldrich *et al.*, 1987; Houghton & Ornston, personal communication). This, together with observed similarities in molecular weight and Mn^{2+} dependence (Kuhm *et al.*, 1990), suggests that CMCI and MCI have a common precursor and that the two enzymes should have some structural similarities. The sequence differences are too large, however, to permit a detailed analysis of the remarkable substrate specificity and the dehalogenating capability at the molecular level from an analysis of MCI alone. We therefore recently crystallized the pJP4-encoded CMCI (Hammer *et al.*, 1993) and report here its three-dimensional structure. We also compare the structure of CMCI with that of MCI in order to explain the altered substrate specificity. The crystal structure of CMCI, in combination with molecular modelling studies, provide a basis for studies of mutant enzymes involving specific amino-acid exchanges that alter the substrate specificity.

```
                    .         .         .         .        50
CMCI      MKIDAIEAVIV-DVPTKRPIQM-SITTVHQQSYVIVRVY-SEGLVGVGEGGSV
MCI     MTSVLIERIEAIIVHDLPTIRPPHKLAMHTMQTQTLVLIRVRCSDGVEGIGEATTI

                    .         .         .         .       100
CMCI      GGPVWSAECAETIKIIVERYLAPHLLGTDAFNVSGALQTMARAVTGNASA
MCI       GGLAYGYESPEGIKANIDAHLAPALVGLPADNINAAMLKLDKLAKGNTFA

                    .         .         .         .       150
CMCI      KAAVEMALLDLKARALGVSIAELLGGPLRSAIPIAWTLASGDTKRDLDSA
MCI       KSGIESALLDAQGKRLGLPVSELLGGRVRDSLEVAWTLASGDTARDIAEA

                    .         .         .         .       200
CMCI      VEMIERRRHNRFKVKLGFRSPQDDLIHMEALSNSLGSKAYLRVDVNQAWD
MCI       QHMLEIRRHRVFKLKIGANPLAQDLKHVVAIKRELGDSASVRVDVNQYWD

                    .         .         .         .       250
CMCI      EQVASVYIPELEALGVELIEQPVGRENTQALRRLSDNNRVAIMADESLST
MCI       ESQAIRACQVLGDNGIDLIEQPISRINRSGQVRLNQRSPAPIMADESIES

                    .         .         .         .       300
CMCI      LASAFDLARDRSVDVFSLKLCNMGGVSATQKIAAVAEASGIASYGGTMLD
MCI       VEDAFSLAADGAASIFALKIAKNGGPRAVLRTAQIAEAAGIALYGGTMLE

               RLHS-AYLRFHASVRLRTV-     .         .       350
CMCI      STIGTSVALQLYSTVPSLPFGCELIGPFVLADTLSHEPLEIRDYELQVPT
MCI       GSIGTLASAHAFLTLRQLTWGTELFGPLLLTEEIVNEPPQYRDFQLHIPR

                    .       370
CMCI      GVGHGMTLDEDKVRQYARVS
MCI       TPGLGLTLDEQRLARFARR
```

Fig. 3. Alignment of the amino-acid sequences of chloromuconate cycloisomerase (CMCI) from *Alcaligenes eutrophus* JMP134 (Perkins *et al.*, 1990) and of muconate cycloisomerase (MCI) from *Pseudomonas putida* (Aldrich *et al.*, 1987), as predicted from the corresponding DNA sequences. The amino-terminal amino acid of chloromuconate cycloisomerase was determined by protein sequencing (Hammer *et al.*, 1993). Positions identical in both sequences are connected by vertical lines. Shown above positions 306–325 (underlined) of chloromuconate cycloisomerase is the sequence reported for this region by Ghosal & You (1989). At the DNA level the differences correspond to six missing bases at positions 916, 927, 932, 937, 949 and 973.

Materials and methods

Chemicals and crystallization

Chemicals and buffers were purchased from Merck (Darmstadt, Germany), Fluka (Neu-Ulm, Germany), Sigma (Deisenhofen, Germany) or Serva (Heidelberg, Germany). The purification of the enzyme CMCI has been described elsewhere (Kuhm *et al.*, 1990; Hammer, 1989).

For crystallization (Hammer *et al.*, 1993) the protein concentration was adjusted to 8–9 mg ml^{-1} by ultrafiltration in Centricon 10 microconcentrators (Amicon). The protein solution was dialyzed overnight at 280 K against 5 m*M* Tris hydrochloride pH 7.3 containing 2 m*M* $MnSO_4$. All buffers/precipitant solutions contained 0.02% NaN_3 and 2 m*M* $MnSO_4$ in addition to the components given below.

Crystals were grown by the hanging-drop method (McPherson, 1982). Drops were made by mixing 3 μl of protein solution with 3 μl of bottom liquid consisting of 0.3 *M* $(NH_4)_2SO_4$, 0.1 *M* cacodylate, 30% (*w*/*w*) PEG 8000, pH 6.5 at 280 K. The reservoir was filled with 1 ml of precipitant solution. The tetragonal bipyramidal crystals reached 0.5 mm along each edge after 4–6 weeks.

Data collection and processing

X-ray diffraction data were measured on two crystals with a Siemens X100A area detector mounted on a Siemens XP12 rotating-anode generator, running at 40 kV and 100 mA to produce graphite-monochromatized Cu *Kα* radiation. The detector was set at 15 cm from the crystal at $2\theta = 17.5°$. Data were measured in ω oscillations with 0.2° $frame^{-1}$; exposure time was 60 s $frame^{-1}$. The temperature was maintained at 295 K. For data processing the *XENGEN* program suite (Howard *et al.*, 1987) was used. The data set merged from two crystals was truncated at 3.0 Å. At this resolution 48 931 measurements contributed to 18 204 unique reflections (fraction collected 99.4%, $R_{merge}(I) = 10.1\%$ for all data). Beyond this resolution data were judged insignificant because of low intensity [$\langle I/\sigma(I)\rangle < 2.2$] and a high *R* value of 32.2%. In addition, the reflections collected beyond 3 Å resolution were incomplete. On the basis of Laue symmetry and systematic absences crystals were assigned to the tetragonal space group *I*4, with unit-cell dimensions $a = b = 111.89$, $c = 148.49$ Å, and with two monomers, molecular mass 40 kDa, per asymmetric unit (for summary, see Table 1). The volume per unit weight, 2.99 $Å^3\ Da^{-1}$, lies well within the range of values compiled by Matthews (1968). This packing allows the protein to be present in the crystal as an octamer, in agreement with biochemical data (Kuhm *et al.*, 1990).

Table 1. *Summary of data collected from CMCI crystals*

Number of crystals	2
Resolution range (Å)	20.0–3.0
Total observations	48 931
Unique reflections	18 204
Possible reflections	18 311
Completeness (%)	99.4
$R_{merge}(I)$* (%)	10.1
Space group	*I*4
Cell dimensions (Å)	$a = b = 111.89$, $c = 148.49$

*$R_{merge}(I) = \sum_i (I_i - \bar{I})/\sum_i I_i$.

Structure determination

The crystal structure of CMCI was determined by molecular-replacement techniques by the use of the atomic coordinates of MCI from *Pseudomonas putida* (Goldman A., unpublished work). The *MERLOT* program suite (Fitzgerald, 1988) was used for the molecular-replacement studies. The self-rotation search revealed non-crystallographic two-fold symmetry. MCI had also crystallized as an octamer with a dimer of two identical subunits per asymmetric unit. Consequently, rotation and translation searches were performed using only the backbone atoms of this dimer and diffraction data between 8.0 and 4.0 Å resolution. Rotation searches were also performed with all the atoms of the dimer and with the monomer. These did not, however, result in correct solutions. The cross-rotation function that used the backbone atoms of the dimer had a major peak at $\alpha = 71.25$, $\beta = 87.00$, $\gamma = 90.00°$ and was refined to $\alpha = 71.79$, $\beta = 86.50$, $\gamma = 88.67°$. This peak and the one for its symmetry-related counterpart were the highest peaks in the rotation function at 25σ significance level. No other set of peaks exceeded 65% of their value. The solution of the translation function, calculated from the highest peak, was at $x = 0.988$, $y = 0.001$. The *R* value for this solution was $R = 51.4\%$ from backbone atoms. No crystal contacts with symmetry-related molecules were found at a distance < 3 Å and only eight at a distance < 4 Å.

A polyalanine model of CMCI was placed into the unit cell accordingly. Side chains were fitted by use of the computer program *FRODO* (Jones, 1978) into a $2F_o - F_c$ map computed with data in the resolution range of 20.0–3.0 Å. At this early stage of structure determination, the amino-acid sequence of the protein was not known precisely, since corresponding reports from two different research groups (Ghosal & You, 1989; Perkins *et al.*, 1990) varied in several positions near the C-terminal end (Fig. 3). After adding side chains to the model in periodically recalculated $2F_o - F_c$ maps, the sequence reported by Perkins *et al.* (1990) was determined to be correct. For the alternative sequence, side chains of residues

306–325 could not be fitted into the electron density. In this way, all amino acids of subunit I had been fitted except those of the carboxy- and amino-terminal ends as well as some amino acids in loop regions where electron density was difficult to interpret and residues 18–26 which had not been included in the initial model. This subunit was superimposed onto the backbone of the other to generate the second subunit by transferring side chains. The model of the dimer created by this method was refined to $R = 48.8\%$ by restrained least-squares techniques using the computer program *PROLSQ* (Hendrickson & Konnert, 1980). At this stage, refinement was continued by the method of simulated annealing using the computer program *X-PLOR* (Brünger, Karplus & Petsko, 1989) and the R value dropped to $R = 26.3\%$. The simulated-annealing run followed a fast-cool protocol (Table 2). Afterwards several subsequent cycles of positional least-squares refinement, with a fixed isotropic temperature factor of 25 Å^2 were carried out for data in the resolution range of 12.0–3.0 Å. At this stage of refinement, the electron density for residues 18–26 could be clearly seen in omit maps. This part of the enzyme structure was first modeled as a polyalanine loop and refined by simulated annealing; then side chains were fitted into the electron-density map. In addition, amino acids with incorrect geometry had been adjusted by use of omit maps. After further positional refinement and some cycles of temperature-factor refinement with *X-PLOR*, in which both molecules were treated independently, the structure converged at $R = 19.5\%$. The data used for this refinement had intensities above 3σ and lay in the resolution range 8.0–3.0 Å. No restraints on non-crystallographic symmetry were applied during any of the refinement steps. The temperature factors of main-chain atoms ranged from $B = 5$ to 65 Å^2 (Fig. 4), while those of side-chain atoms lay between $B = 2$ and 65 Å^2; the minimum value set by the program is 2 Å^2.

Table 2. *Fast-cooling simulated-annealing protocol*

Relaxing stage	
Tolerance (Å)	0.05
Integration steps	40
Annealing stage	
(*a*) Heat stage	
Temperature (K)	2000
Integration steps	1000
Integration time step (ps)	0.001
Tolerance (Å)	0.2
(*b*) Cool stage	
Temperature (K)	300
Integration steps	250
Integration time step (ps)	0.001
Tolerance (Å)	0.2
Final stage	
Tolerance (Å)	0.05
Integration steps	40

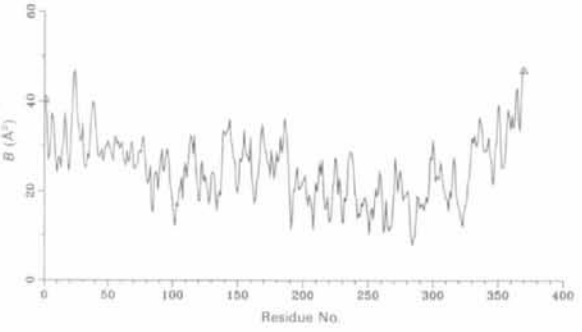

Fig. 4. Main-chain *B*-factor plot of subunit I. The temperature-factor distribution of subunit II is similar and not shown here.

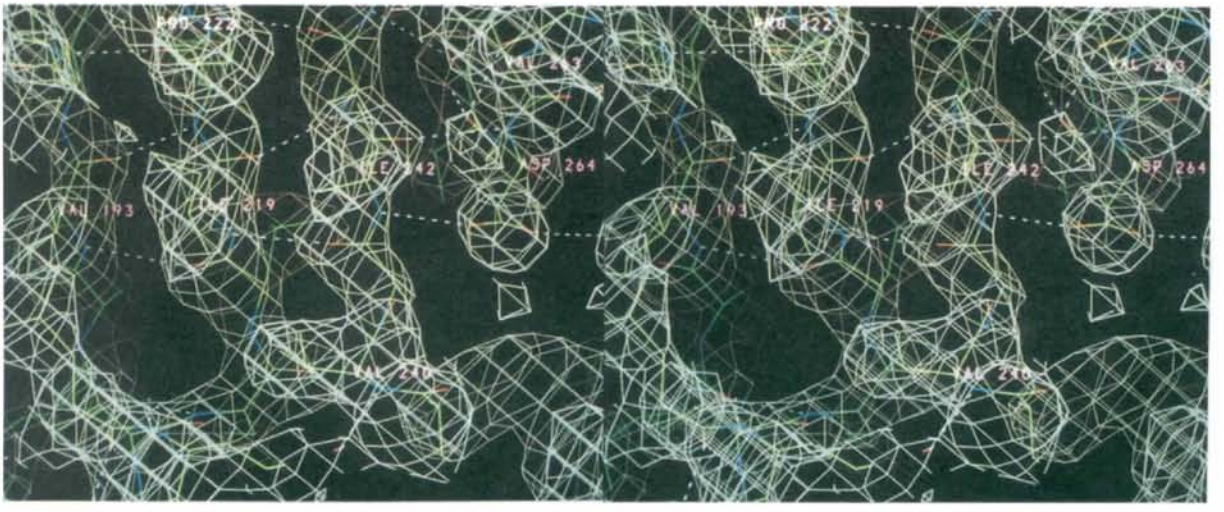

Fig. 5. Portion of the hydrophobic surface of the β-barrel of CMCI with $(2F_o - F_c)$ electron density contoured to 1σ above the mean.

A typical $2F_o - F_c$ map, calculated with data in the resolution range 20.0–3.0 Å after structure refinement, is shown in Fig. 5.

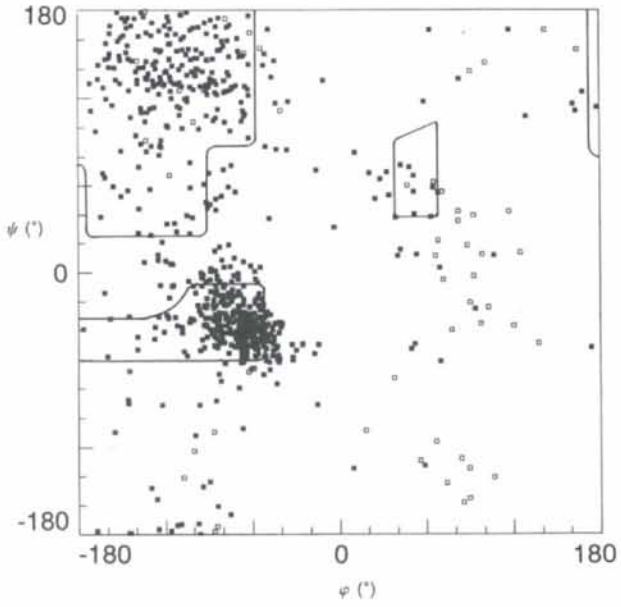

Fig. 6. Ramachandran plot for both molecules per asymmetric unit. Glycines are plotted as open squares, all other residues as full squares.

The coordinates have been deposited with the Brookhaven Protein Data Bank, from which they are available upon request.*

Results and discussion

Refinement results

In the final model of CMCI, the root-mean-square (r.m.s.) deviations from ideal bond lengths and angles (of all non-H atoms) are 0.029 Å and 5.066°, respectively. The two monomers in the asymmetric unit are not totally identical. After least-squares superposition, the r.m.s. deviations are 0.863 Å for backbone atoms and 1.542 Å for all non-H atoms. In addition, Arg17 in subunit I as well as Glu179, Arg239 and Arg368 in subunit II were found to be disordered, since the electron density for these residues revealed two possible side-chain conformations. After refinement the temperature factors for these residues ranged from $B = 19$ to 44 Å^2, which were similar to those of the neighboring residues. Devia-

* Atomic coordinates and structure factors have been deposited with the Protein Data Bank, Brookhaven National Laboratory (Reference: 1CHR, R1CHRSF). Free copies may be obtained through The Technical Editor, International Union of Crystallography, 5 Abbey Square, Chester CH1 2HU, England (Supplementary Publication No. SUP 37099). A list of deposited data is given at the end of this issue.

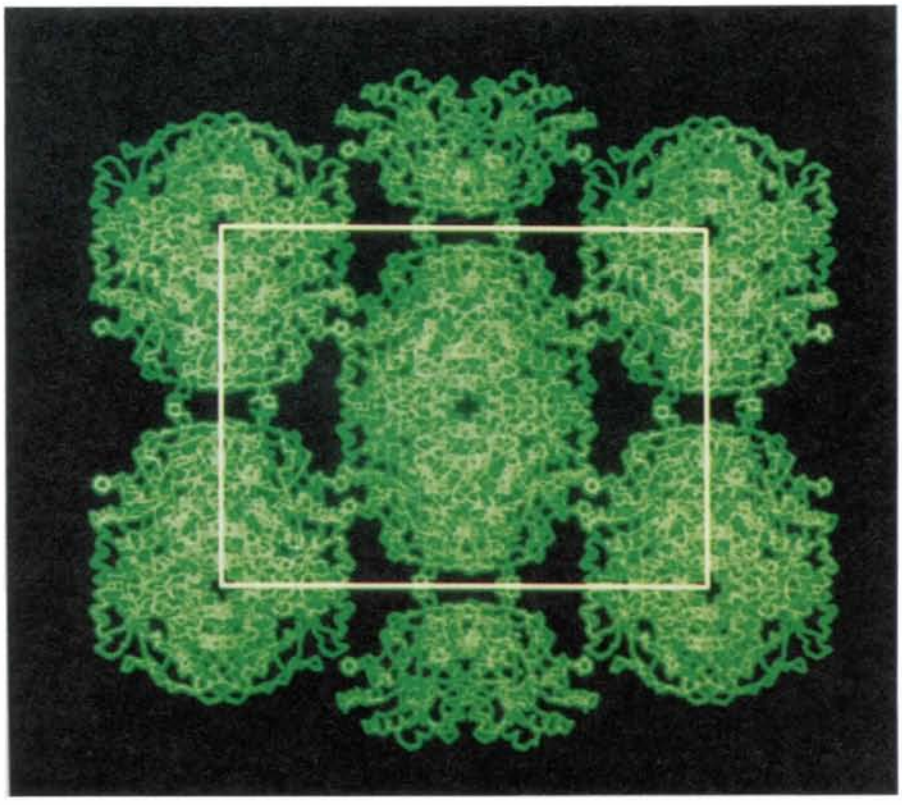

Fig. 7. Crystal packing of chloromuconate cycloisomerase. The protein is represented as a Cα trace.

tions in bond lengths of backbone atoms greater than 0.06 Å from ideal values were mainly found between residues 18 and 44 in two loops and near the C-terminal end. High temperature factors (> 35 Å^2) for main-chain atoms were mostly found in the same regions.

Analysis of the results using the method of Luzzati (1952) indicates that the r.m.s. error in coordinates is about 0.3 Å.

A Ramachandran plot (Ramachandran, Ramakrishnan & Sasisekharan, 1963) of the backbone torsion angles is shown in Fig. 6. Most of the residues outside the allowed regions are located in turns or sheets, and they tend to return to this position after manual adjustment and subsequent refinement. Those residues which were located in helical regions could be adjusted by this procedure.

Crystal packing and quaternary structure

CMCI from *Alcaligenes eutrophus* JMP134 is present as an octamer with two subunits per asymmetric unit, related by a non-crystallographic twofold axis. Thus, two octamers fill the unit cell. Each of the eight subunits consists of 370 amino acids and binds one manganese ion.

In the crystal structure the octameric protein molecules are located on the corners and in the center of

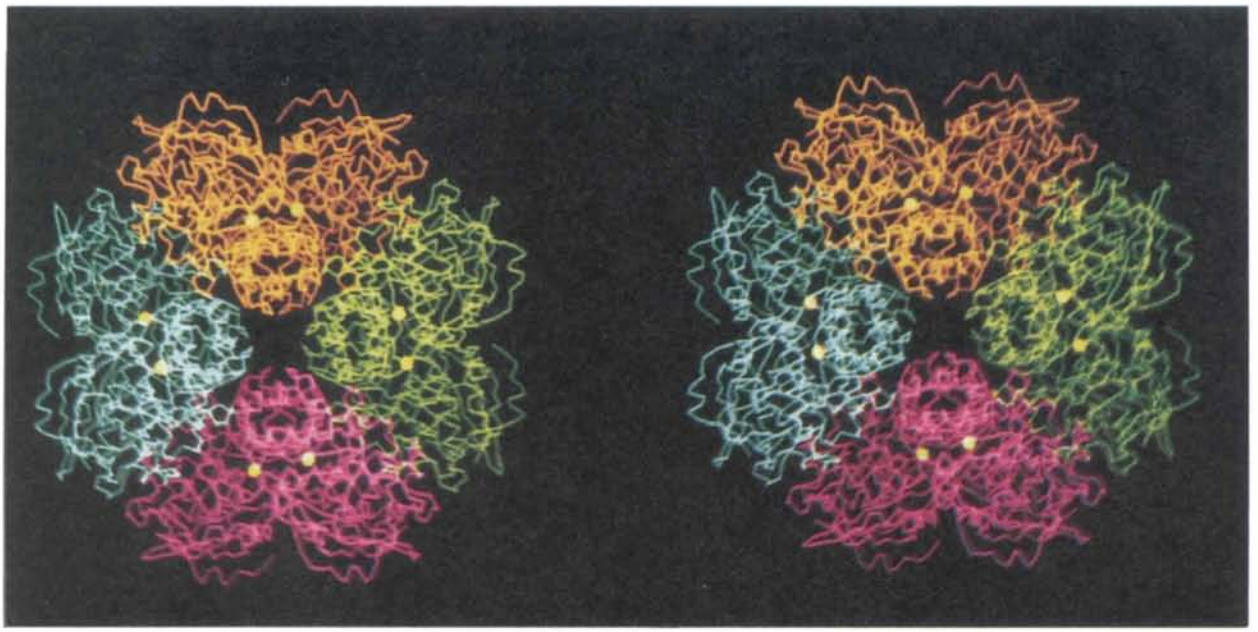

Fig. 8. Stereoview of the octameric enzyme represented as a Cα carbon trace. The four dimers, created by the crystallographic fourfold symmetry are drawn in different colors. Manganese ions are drawn with their van der Waals surfaces.

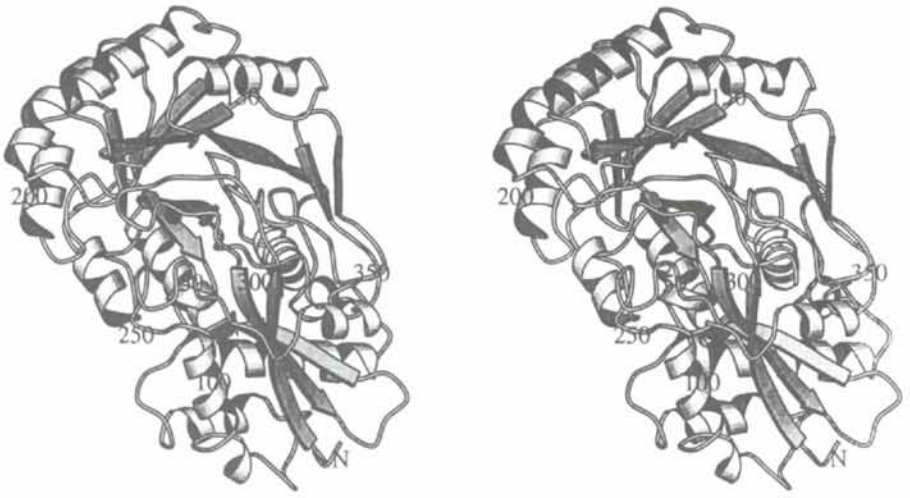

Fig. 9. Schematic stereo drawing of a CMCI subunit. β-strands are drawn as arrows, α-helices as wound ribbons and the Mn^{2+} ion as solid sphere. The separation in two structural domains is clearly revealed in this orientation. Prepared with *MOLSCRIPT* (Kraulis, 1991).

the unit cell (Fig. 7). There are only few regions where the octamers are in close contact with their neighbors. Among these regions are the short C-terminal helices (residues 360–365) which are stacked on top of each other. The amino- and carboxy-terminal ends are located on the surface of the assembly, and in the monomer they are 32 Å apart.

Fig. 8 shows details of the octamer architecture which indicates C_4 point-group symmetry as a result of the differences found between the two subunits in the asymmetric unit. The coarse overall shape, however, can be approximated by D_4 point-group symmetry. A channel along the fourfold axis leads through the middle of the complex. In this area an exceptionally large number of charged residues are found.

The active site with the bound manganese ion can be easily reached by the substrate from the surface of the octamer through a cleft between two subunits.

As a result of the non-crystallographic symmetry there are different contacts between the subunits in the octamer. Like in MCI the packing around the twofold axis is tighter than that around the fourfold axis. In the latter case two helices (residues 251–258 and 276–289) in the barrel domain of subunit I make contact with the equivalent helices of subunit II in the other asymmetric unit. Further pairwise contacts between different asymmetric units were found between the N-terminus of the second and the C-terminus of the fourth helix in domain I. In addition Gly290, located in a loop, lies close to the N-terminus of a barrel helix (residues 203–212) in the other subunit.

The closest molecular packing, however, is found for the two monomers related by a non-crystallographic twofold axis. In this case the first helix of domain I in both subunits makes close contacts as well as Pro53 and Thr95 which are located in loops.

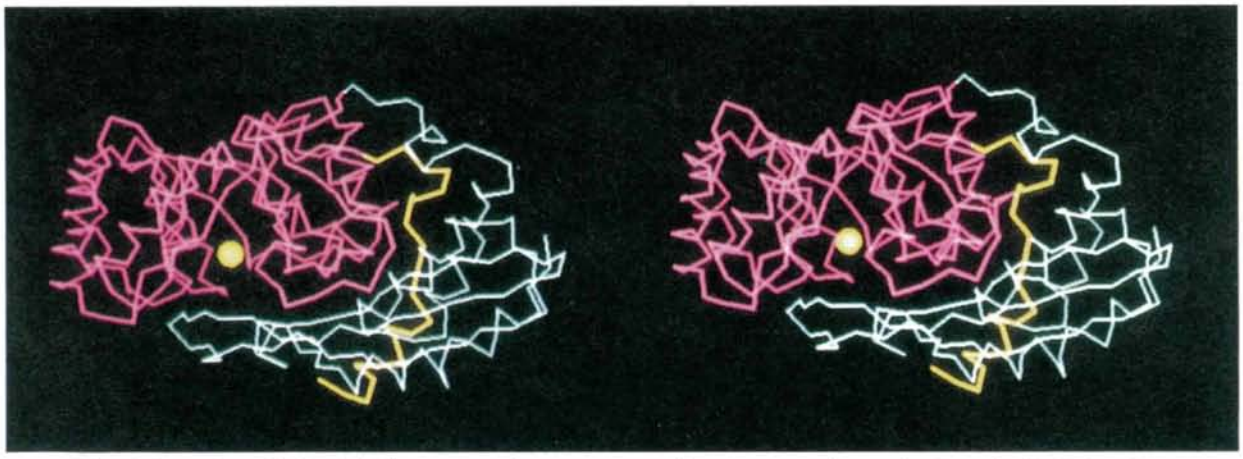

Fig. 10. Stereoview of subunit I. The two domains are represented in magenta and cyan; the C-terminal helix in yellow.

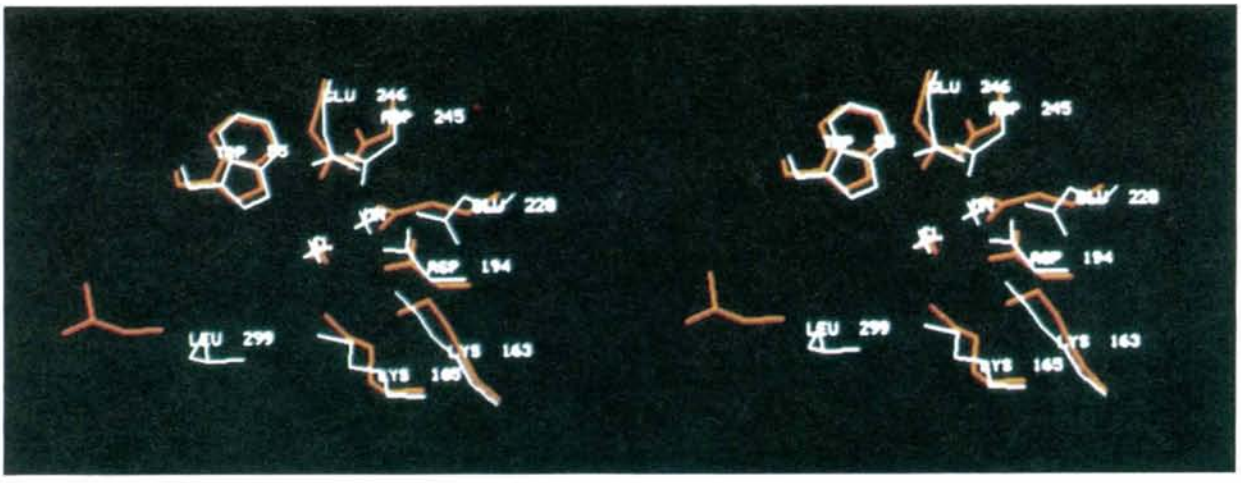

Fig. 11. Stereoview into the active site of CMCI. Subunit I is shown in cyan and subunit II in red.

There are several potential hydrogen bonds and salt bridges that serve to stabilize a compact assembly.

Structure of the monomer

The monomer of CMCI consists of two large domains and one small C-terminal helix, similar to MCI (Goldman *et al.*, 1987). A schematic representation is shown in Fig. 9. Domain I starts with a three-stranded antiparallel β-sheet followed by three long α-helices and one short helix. A long extended strand (residues 131–138) connects this domain with the second (domain II) which is an α/β-barrel, showing a $(\beta\alpha)_7$ motif. Thus, CMCI belongs to the large group of α/β-barrel proteins like xylose isomerase, mandelate racemase or triose phosphate isomerase (Carrell, Rubin, Hurley & Glusker, 1984; Farber & Petsko, 1990; Neidhart, Kenyon, Gerlt & Petsko, 1990; Banner *et al.*, 1975). The last four residues (135–138) of the strand mentioned above are part of the barrel, while the first three residues (131–133) belong to a short three-stranded antiparallel β-pleated sheet completed by residues 340–342 and 345–347. A long chain connecting the last helix of the $(\beta\alpha)_7$ motif with this short β-sheet seems to be part of the central barrel core, but only one potential hydrogen-bond bridge to residue 134 is found in this 3 Å resolution protein model. Domain I lies at the side of the α/β-barrel and covers part of its base. Finally, the C-terminal helix comes out of a cleft between the two large domains and is involved in crystal packing as described above. The manganese ion is located at the base of the barrel (Fig. 10).

Residues 18–26, which could not be located in the crystal structure of MCI, form a large loop also covering part of the barrel near the site where Mn^{2+} is bound. The weak electron density and large temperature factors between residues 23 and 25 as well as a different tracing of these residues in subunits I and II indicate the high flexibility of this structural element.

Active-site structure

Between domains I and II there is a channel leading to the active site where the Mn^{2+} is located. Inside this channel there are several positively charged groups (Arg17, Lys163, Lys165, Arg225 and Lys269), while the back of the catalytic center is dominated by negatively charged side chains (Asp194, Glu220, Asp245, Glu246 and Glu323). In addition, this region between the two domains contains several uncharged polar residues. Although the two subunits per asymmetric unit are related by non-crystallographic symmetry, significant structural differences are present at the active sites. Both active sites of the asymmetric unit show a strong electron-density maximum surrounded by negatively charged side chains which was assigned as the active Mn^{2+} atom in accordance with the biochemical data (Kuhm *et al.*, 1990). The temperature factors of these cations, 23 $Å^2$ in subunit I and 24 $Å^2$ in subunit II, are close to those of the protein atoms to which they are bound.

In the first subunit, an electron-density maximum was found next to Mn^{2+} at a distance of 2.6 Å which was not observed in the second subunit in any difference electron-density map. There is some evidence that this density represents a chloride ion. Filling this position with a water oxygen or other molecules or ions, used during purification and crystallization, inevitably resulted in large positive or negative difference electron density and abnormal temperature factors. Chloride fitted best, giving a B value of 24 $Å^2$. In addition, the $Mn^{2+}\cdots Cl^-$ distance of 2.6 Å is well within the range found in the Cambridge Structural Database (Allen *et al.*, 1991) for Mn^{2+}/Cl^- pairs. In the second subunit, Mn^{2+} is located close to the place where Cl was found in the first subunit. A comparison of the active sites of both molecules (Fig. 11) shows major differences in the side-chain conformations of Asp194, Glu220, Asp245, Glu246, Leu299 and Glu323. In subunit I, the cation is coordinated by Asp194, Glu220, Asp245 and Cl . The distance of 1.8 Å between Mn^{2+} and the oxygen of Asp245 involved in metal coordination is extremely short (values usually range between 2.10 and 2.30 Å), and Mn^{2+} is located deeper in the barrel than in the subunit without chloride. In subunit II where Mn^{2+} is located at a different place and no chloride was found, the cation is coordinated by the same amino acids as found in subunit I, yet the $Mn^{2+}\cdots O$ distances range from 2.7 to 3.8 Å. This may indicate the presence of water in an inner coordination sphere that cannot be located at this resolution.

If the chloride ion is regarded as a substitute for the substrate, these results may give us some information on any conformational changes in the active site that might involve substrate binding. These include side-chain rotations as well as a movement of the metal ion deeper into the pocket.

Comparison with the crystal structure of muconate cycloisomerase

As expected from the high sequence similarity , the folding of CMCI is generally similar to that of MCI, meanwhile determined at 1.8 Å resolution (Goldman, unpublished work). Despite overall backbone similarities, there are remarkable differences in the channel leading to the active site and within the catalytic center. In MCI this channel is narrowed by tyrosine residues (Tyr55, Tyr57 and Tyr198). In the case of CMCI they are replaced by Trp55, Ala57 and

Ala198. In addition the inner part of the channel shows a different curvature which is circular in cross-section and more bent in CMCI than in MCI where the channel has an oval shape. Thus, the substrate reaches the active centre from a slightly different direction (about 15°) in the two different enzymes.

A remarkable change is seen in the side chain of Trp55. In spite of the fact that in both enzymes the residues in this position are situated at the entrance of the active site, Trp55 in CMCI is found to be located in a different place than the corresponding tyrosine in MCI. As a result more space for a substrate is available despite the larger volume of this amino acid.

As a result of the missing polypeptide residues 18–26 in the crystal structure of MCI, which, in CMCI, form a large loop covering part of the base of the α/β-barrel, a more detailed comparison of the outer part of the channel cannot be carried out. For CMCI this structural element is shorter and less polar. It possibly plays a role in substrate pre-selection or substrate orientation.

Conformational changes caused in the active site by five amino-acid exchanges between MCI and CMCI (Val50, Trp55, Ser267, Ile325 and Val329) are responsible for widening this area in CMCI and may enable docking of larger molecules in a different position. In addition, Mn^{2+} in MCI is located at the position where the chloride-coordinated cation in subunit I is found in CMCI.

Thus, conformational changes as well as changes in polarity and size of the channel leading to the active site may be responsible for the observed variation in substrate specificity.

We thank Martin D. Vollmer for protein purification. This work was supported by a grant from the Bundesministerium für Forschung und Technologie (Projekt A10U, Zentrales Schwerpunktprojekt Bioverfahrenstechnik, Stuttgart) and by grant CA 10925 from the National Institutes of Health.

References

ALDRICH, T. L., FRANTZ, B., GILL, J. F., KILBANE, J. J. & CHAKRABARTY, A. M. (1987). *Gene*, **52**, 185–195.

ALLEN, F. H., DAVIES, J. E., GALLOY, J. J., JOHNSON, O., KENNARD, O., MACRAE, C. F., MITCHELL, E. M., MITCHELL, G. F., SMITZ, J. M. & WATSON, D. G. (1991). *J. Chem. Inf. Comput. Sci.* **31**, 187–204.

AVIGAD, G. & ENGLARD, S. (1969). *Fed. Proc. Fed. Am. Soc. Exp. Biol.* **28**, 345.

AVIGAD, G., ENGLARD, S., OLSEN, B. R., WOLFENSTEIN-TODEL, C. & WIGGINS, R. (1974). *J. Mol. Biol.* **89**, 651–662.

BANNER, D. W., BLOOMER, A. C., PETSKO, G. A., PHILLIPS, D. C., POGSON, C. I. & WILSON, I. A. (1975). *Nature (London)*, **255**, 609–614.

BRÜNGER, A. T., KARPLUS, M. & PETSKO, G. A. (1989). *Acta Cryst.* A**45**, 50–61.

CARRELL, H. L., RUBIN, B. H., HURLEY, T. J. & GLUSKER, J. P. (1984). *J. Biol. Chem.* **259**, 3230–3236.

DORN, E. & KNACKMUSS, H.-J. (1978). *Biochem J.* **174**, 85–94.

ENGESSER, K. H. & FISCHER, P. (1991). *Biodegradation: Natural and Synthetic Materials*, edited by W. B. BETTS, pp. 15–54. London: Springer-Verlag.

FARBER, G. K. & PETSKO, G. A. (1990). *Trends Biochem. Sci.* **15**, 228–234.

FITZGERALD, P. M. D. (1988). *J. Appl. Cryst.* **21**, 273–278.

GHOSAL, D. & YOU, I.-S. (1989). *Gene*, **83**, 225–232.

GOLDMAN, A., OLLIS, D. L. & STEITZ, T. A. (1985). *J. Mol. Biol.* **182**, 353–355.

GOLDMAN, A., OLLIS, D. L. & STEITZ, T. A. (1987). *J. Mol. Biol.* **194**, 143–153.

HÄGGBLOM, M. M. (1992). *FEMS Microbiol. Rev.* **103**, 29–72.

HAMMER, A. (1989). Diplomarbeit, Univ. Stuttgart, Germany.

HAMMER, A., HILDENBRAND, T., HOIER, H., NGAI, K.-L., SCHLÖMANN, M. & STEZOWSKI, J. J. (1993). *J. Mol. Biol.* **232**, 305–307.

HENDRICKSON, W. A. & KONNERT, J. H. (1980). *Computing in Crystallography*, edited by R. DIAMOND, S. RAMASESHAN & K. VENKATESAN, pp. 13.01–13.25. Bangalore: Indian Academy of Sciences.

HOWARD, A. J., GILLILAND, G. L., FINZEL, B. C., POULOS, T. L., OHLENDORF, D. H. & SALEMME, F. R. (1987). *J. Appl. Cryst.* **20**, 383–387.

JONES, T. A. (1978). *J. Appl. Cryst.* **11**, 268–272.

KOZARICH, J. W., CHARI, R. V. J., NGAI, K.-L. & ORNSTON, L. N. (1986). *Mechanisms of Enzymatic Reactions: Stereochemistry*, edited by P. A. FREY, pp. 233–246. New York: Elsevier.

KRAULIS, P. J. (1991). *J. Appl. Cryst.* **24**, 946–950.

KUHM, A. E., SCHLÖMANN, M., KNACKMUSS, H.-J. & PIEPER, D. H. (1990). *Biochem. J.* **266**, 877–883.

LUZZATI, V. (1952). *Acta Cryst.* **5**, 802–810.

MCPHERSON, A. (1982). *The Preparation and Analysis of Protein Crystals*. New York: John Wiley.

MATTHEWS, B. W. (1968). *J. Mol. Biol.* **33**, 491–496.

NEIDHART, D. J., KENYON, G. L., GERLT, J. A. & PETSKO, G. A. (1990). *Nature (London)*, **347**, 692–694.

NGAI, K.-L. & KALLEN, R. G. (1983). *Biochemistry*, **22**, 5231–5236.

PERKINS, E. D., GORDON, M. P., CACERES, O. & LURQUIN, P. F. (1990). *J. Bacteriol.* **172**, 2351–2359.

PIEPER, D. H., KNACKMUSS, H.-J. & TIMMIS, K. N. (1993). *Appl. Microbiol. Biotechnol.* **39**, 563–567.

PIEPER, D. H., REINEKE, W., ENGESSER, K.-H. & KNACKMUSS, H.-J. (1988). *Arch. Microbiol.* **150**, 95–102.

RAMACHANDRAN, G. N., RAMAKRISHNAN, C. & SASISEKHARAN, V. (1963). *J. Mol. Biol.* **7**, 955–999.

SCHLÖMANN, M. (1992). *Biologischer Abbau von Chlorkohlenwasserstoffen – Biologische Abwasserreinigung*, Vol. 1, edited by B. WEIGERT, pp. 87–109. Berlin: Verlag Technische Univ.

SCHLÖMANN, M., FISCHER, P., SCHMIDT, E. & KNACKMUSS, H.-J. (1990). *J. Bacteriol.* **172**, 5119–5129.

SCHMIDT, E. & KNACKMUSS H.-J. (1980). *Biochem. J.* **192**, 339–347.

VOLLMER, M. D. & SCHLÖMANN, M. (1993). *Bioengineering*, **9**, 55.